





Observing Scenarios for the Next Decade of Early Warning Detection of Binary Neutron Stars

Ryan Magee¹  and Ssohrab Borhanian² ¹ LIGO, California Institute of Technology, Pasadena, CA 91125, USA² Theoretisch-Physikalisches Institut, Friedrich-Schiller-Universität Jena, D-07743 Jena, Germany

Received 2022 January 31; revised 2022 May 31; accepted 2022 July 5; published 2022 August 23

Abstract

We describe representative observing scenarios for early warning detection of binary neutron star mergers with the current generation of ground-based gravitational wave detectors as they approach design sensitivity. We incorporate recent estimates of the infrastructure latency and detector sensitivities to provide up-to-date predictions. We use Fisher analysis to approximate the associated localizations, and we directly compare to Bayestar to quantify biases inherited from this approach. In particular, we show that Advanced LIGO and Advanced Virgo will detect and distribute $\lesssim 1$ signal with signal-to-noise ratio greater than 15 before a merger in their fourth observing run provided they maintain a 70% duty cycle. This is consistent with previous early warning detection estimates. We estimate that 60% of all observations and 8% of those detectable 20 s before a merger will be localized to $\lesssim 100 \text{ deg}^2$. If KAGRA is able to achieve a 25 Mpc horizon, 70% of these binary neutron stars will be localized to $\lesssim 100 \text{ deg}^2$ by a merger. As the Aundha–Hanford–KAGRA–Livingston–Virgo network approaches design sensitivity over the next ~ 10 yr, we expect one (six) early warning alerts to be distributed 60 (0) s before a merger. Although adding detectors to the Hanford–Livingston–Virgo network at design sensitivity impacts the detection rate at $\lesssim 50\%$ level, it significantly improves localization prospects. Given uncertainties in sensitivities, participating detectors, and duty cycles, we consider 103 future detector configurations so electromagnetic observers can tailor preparations toward their preferred models.

Unified Astronomy Thesaurus concepts: Neutron stars (1108); Compact objects (288); Gravitational wave astronomy (675); Gravitational waves (678); Time domain astronomy (2109); Transient sources (1851)

Supporting material: animation

1. Introduction

Advanced LIGO (Aasi et al. 2015), Advanced Virgo (Acernese et al. 2015), and KAGRA (Akutsu et al. 2019) have enjoyed remarkable success since the first detection of gravitational waves (GWs) from a binary black hole merger in 2015 (Abbott et al. 2016). Since then, analyses by the LIGO–Virgo–KAGRA Collaboration (LVK) have uncovered a growing population of binary black holes, binary neutron stars (BNSs), and neutron star–black hole binaries (NSBHs; Abbott et al. 2019, 2021a, 2021b, 2021c). Analyses of public data (Trovato 2020) have confirmed many of these detections and hinted at other promising candidates lurking deeper in the noise (Magee et al. 2019; Nitz et al. 2019; Zackay et al. 2019; Nitz et al. 2020b; Venumadhav et al. 2020; Nitz et al. 2021; Olsen et al. 2022).

GW observations coincident with other astrophysical signals such as electromagnetic radiation or particles are a highly sought-after subclass of so-called *multimessenger* detections. Even before the first detection of GWs, various studies investigated what to expect from electromagnetic follow-up efforts during the Advanced LIGO and Advanced Virgo era (Cannon et al. 2012; Singer et al. 2014). The first multimessenger detection with GWs, GW170817 (Abbott et al. 2017a, 2017b), was serendipitous in nature, and led to

an explosion in works focused on facilitating additional discoveries.

In particular, there has been an increasing focus on *early warning* (or premerger) detection and localization of BNSs and NSBHs (Nitz et al. 2020a; Sachdev et al. 2020; Kovalam et al. 2022; Singh et al. 2021; Tsutsui et al. 2022; Yu et al. 2021). Several of these works, in particular (Chu et al. 2016; Nitz et al. 2020a; Sachdev et al. 2020; Kovalam et al. 2022; Singh et al. 2021), focus on BNS detection for the current generation of ground-based detectors, though many optimistically assume a 100% duty cycle and sensitivities that may prove difficult to reach (Akutsu et al. 2019; Washimi et al. 2021). More recently, there has also been a focus on the infrastructure necessary to realize early warning alerts with an emphasis on latencies expected in the LVK’s fourth observing run (O4; Magee et al. 2021).

In this study, we investigate projected observing scenarios of current generation ground-based detectors for early warning detection using well-established Fisher analysis techniques (Finn 1992; Finn & Chernoff 1993; Cutler & Flanagan 1994; Poisson & Will 1995; Balasubramanian et al. 1996). We extend previous studies in four major ways. First, we directly compare the Fisher technique to the *bayestar* localization algorithm to quantify biases in this work, but also other early warning studies (Chan et al. 2018; Singh et al. 2021; Borhanian & Sathyaprakash 2022; Li et al. 2022) and next generation trade studies (Evans et al. 2021). Second, we estimate the localization for 103 combinations of detectors and detector sensitivities for Advanced LIGO, Advanced Virgo, and KAGRA in O4 as well as at their projected *design* sensitivity (referred to as O5). Third, we provide the probability density distributions of the 90%

credible sky area as a function of early warning time to enable the consideration of arbitrary network combinations, duty factors, and early warning detection times. We compare our results to similar work previously carried out (Nitz et al. 2020a; Abbott et al. 2020b; Sachdev et al. 2020). Finally, we include the impact that the KAGRA detector would have at three projected and one realized sensitivities in light of recent construction difficulties (Akutsu et al. 2019; Washimi et al. 2021).

2. Methods

Bayesian approaches such as full parameter estimation (Veitch et al. 2015; Ashton et al. 2019) and the `bayestar` code (Singer & Price 2016) are presently used to provide the most accurate localizations possible for compact binary mergers. Although full parameter estimation is accurate, it takes $\mathcal{O}(\text{hr} - \text{days})$; `bayestar` does not sample over the masses or spins of the binary and is able to provide comparable localizations in $\mathcal{O}(1 \text{ s})$ when run in parallel (or $\mathcal{O}(1 \text{ minutes})$ on a single thread).³ Singer et al. (2014) showed that the two methods largely agree with each other.

For large trade studies, Fisher analysis methods are often favored due to their analytical dependence on the gravitational waveform model and the characteristics of the detectors under investigation (locations, geometries, and sensitivities). Hence, they provide a simple and fast way of estimating the information a signal contains on the waveform model’s parameter domain. Here, we use the Fisher analysis-based software package `gwbench` (Borhanian 2021) to benchmark the measurement capabilities of 103 detector network configurations detailed in the next section. Since this study is focused on BNS signals that do not merge in the most sensitive bands of current generation detectors, we consistently employ a simple inspiral waveform model, TaylorF2 (Sathyaprakash & Dhurandhar 1991; Blanchet et al. 1995, 2005; Buonanno et al. 2009) to estimate the expected measurement uncertainties for the following parameters: \mathcal{M} , η , D_L , t_c , ϕ_c , ι , ψ , α , δ over the frequency band 10–1024 Hz. These denote the chirp mass, symmetric mass ratio, luminosity distance, coalescence time, coalescence phase, inclination, polarization angle, R.A., and decl., respectively. Finally, we can estimate the uncertainty in sky localization via the 90% credible sky area following Cutler (1998) and Barack & Cutler (2004) as

$$\Delta\Omega_{90} = 2\pi \ln(10) |\cos \delta| \sqrt{\text{Var}(\alpha)\text{Var}(\delta) - \text{Cov}^2(\alpha, \delta)}, \quad (1)$$

where $\text{Var}(\alpha)$ and $\text{Var}(\delta)$ are the variances of the R.A. and decl., respectively, and $\text{Cov}(\alpha, \delta)$ is the covariance between the R.A. and decl.; there are, however, several limitations to Fisher analysis approaches (Vallisneri 2008; Rodriguez et al. 2013). Most well-known is that they are only valid in the high signal-to-noise ratio (S/N) limit ($\gtrsim 10$ per detector; Vallisneri 2008). In addition to potentially underestimating errors, they have also been shown to overestimate (Rodriguez et al. 2013). Sky localizations produced by Fisher analyses can only be interpreted as an estimate of the overall uncertainty in the measurement. They cannot estimate proximity of regions of probability in the sky. Additionally, they can exhibit multimodal degeneracies (Fairhurst 2009) and scale differently with

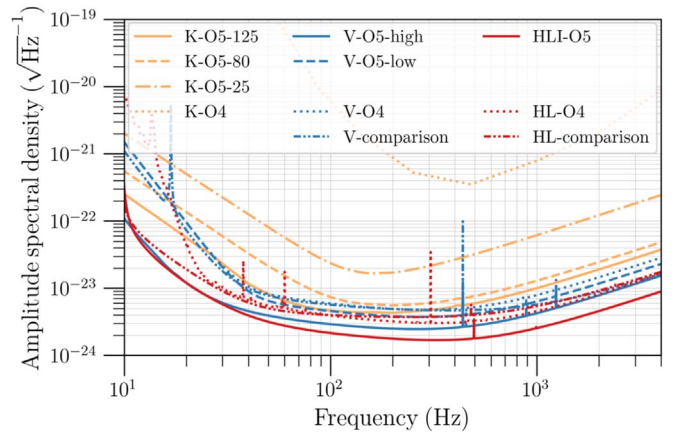


Figure 1. The amplitude spectral densities (ASD) assumed for this trade study. With the exception of the O4 KAGRA ASD that was obtained through digitization of Figure 1 from Washimi et al. (2021); all other ASDs are obtained from the observing scenarios data release. ASDs are labeled as they appear in the data release and/or in the publicly provided estimates in LIGO-T2000012.⁴

the S/N than coherent Bayesian approaches (Berry et al. 2015). As Cannon et al. (2012) noted, Fisher analysis estimates tend to overestimate the uncertainty in localization for low S/N candidates. We quantify this bias of our approach in comparison to `bayestar` in Section 4.1.

We do not impose any single detector S/N thresholds; note that this means low S/Ns in one detector can contribute to the network S/N threshold used as a detection criterion. In practice, we expect the bias introduced by this effect to be small. Unless otherwise noted, we assume a network S/N detection and localization threshold of 15. In all cases, we conservatively assume that no localizations can be provided when only one detector is operating.

3. Population and Networks

Binary neutron star population—Although two probable NSBH systems were recently observed by Advanced LIGO and Advanced Virgo (Abbott et al. 2021d), we restrict the analysis here to BNS populations. Not only does the NSBH population remain uncertain, but their heavier masses mean they pass through the sensitive band of ground-based detectors more rapidly than BNSs. Additionally, only certain mass and spin configurations are conducive to tidally disrupting the neutron star and producing electromagnetic emission (Foucart et al. 2018, 2019). Consequently, their quick evolution, uncertain population, and disruption prospects make them relatively poor early warning detection candidates.

We consider the same astrophysically motivated source population of BNSs as in Sachdev et al. (2020). The source-frame component masses are drawn from a Gaussian distribution with mean mass $1.33 M_\odot$ and standard deviation $0.09 M_\odot$. The source-frame masses are further limited such that $1.0 M_\odot < m_2 < m_1 < 2.0 M_\odot$. This population is modeled after galactic observations of BNSs (Özel and Freire 2016). We note that the masses inferred from GW190425 (Abbott et al. 2020a) are in tension with this population. This could be an indication that galactic measurements are not representative of the broader population of neutron stars. Results from the LVK’s recent

³ See Section 2 of Magee et al. (2021) for a more technical discussion.

⁴ <https://dcc.ligo.org/LIGO-T2000012/public>

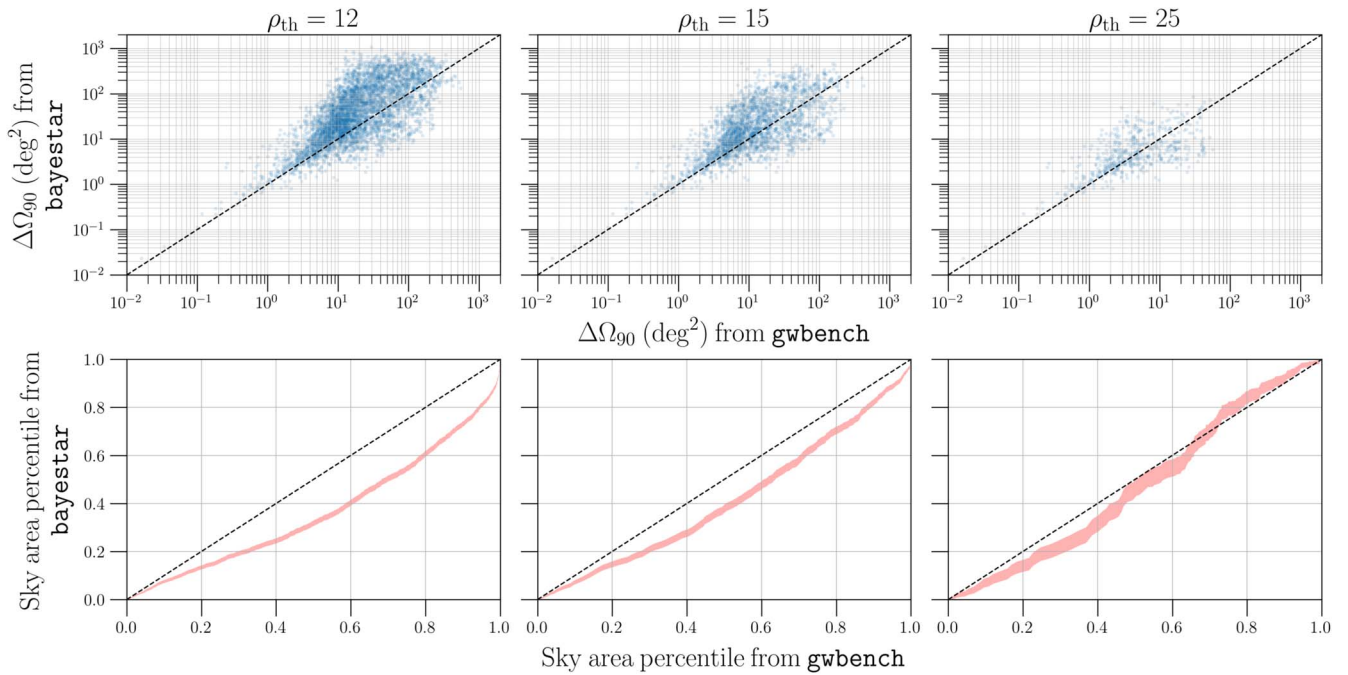


Figure 2. A comparison of the 90% confidence interval computed by *bayestar* vs. the Fisher matrix formalism used here (*gwbench*) for events with network S/N thresholds ρ_{th} of 12, 15, and 25. All localizations are computed assuming a 100% duty cycle and design sensitivity estimates. (Top) Each point represents a localization measurement obtained by both *bayestar* and *gwbench*. Note that the high S/N (small localization) events largely agree, but that this agreement becomes statistical in nature for larger areas. The bias between these two methods is more easily visible in the *pp* plot (bottom) comparing the 90% credible sky area percentiles obtained by *gwbench* and *bayestar*. We include uncertainties on the percentiles measured due to the size of our population, which is dependent on the S/N threshold used. We find that *gwbench* systematically underestimates the size of the confidence interval at S/N 12.

population analysis seem to support this claim (Abbott et al. 2021e). We neglect these uncertainties here and naively apply the most recent BNS merger rate estimates (Abbott et al. 2021e) to our population, though we note that (1) our method can be quickly rerun to produce estimates for arbitrary populations, (2) that as pointed out in Nitz et al. (2020a), our results can be scaled to BNS systems of arbitrary mass, and (3) that expected BNS localizations do not appear to significantly depend on the specifics of the population (Pankow et al. 2020).

Networks—We examine 103 GW detector networks for O4 and O5 that arise from 11 different projected sensitivity curves, summarized in Figure 1. For O4, we consider combinations of Hanford–KAGRA–Livingston–Virgo (HKLTV) networks that contain at least two of the Hanford–Livingston–Virgo (HLV) detectors, with HLV sensitivities as described in the latest observing scenario (LVK 2022). Perhaps the biggest question for O4 is the level to which KAGRA will be able to participate (LVK 2021). In this work, we consider two possible KAGRA sensitivities for O4 with 1 and 25 Mpc BNS detection horizons. We regard this to be a more realistic update to the recent O4 early warning detection and localization estimates provided in Magee et al. (2021), which assumed a horizon of 80 Mpc, especially in light of the recent LVK announcement suggesting KAGRA will start O4 with 1 Mpc horizon (LVK 2021). The O4 KAGRA sensitivity was digitized from Figure 1 in Washimi et al. (2021).

For O5, we consider a five-detector network, Aundha–Hanford–KAGRA–Livingston–Virgo (AHKLV) including LIGO–Aundha (Saleem et al. 2022), previously LIGO–India (Iyer et al. 2011). Following Abbott et al. (2020b), we assume that Aundha, Hanford, and Livingston are all able to achieve comparable sensitivities (e.g., the Advanced LIGO design sensitivity). We compute all network combinations

where at least two of the AHLV detectors are operating. We consider two separate, publicly available sensitivities for Virgo, and three sensitivities for KAGRA, assuming that by O5 KAGRA will achieve either 25, 80, or 125 Mpc BNS detection horizons outlined in the observing scenarios review.

4. Results

4.1. Comparison to Known Localizations

In order to quantify any biases introduced by the Fisher analysis, we compare our localization estimates from *gwbench* to those computed by *bayestar* for all simulated signals recovered by the full search presented in Sachdev et al. (2020). Figure 2 shows a comparison of the 90% credible sky area computed via each method at three network S/N thresholds ρ_{th} (top), together with a *pp* plot comparing the percentiles associated with each localization estimator (bottom). In general, we find that *gwbench* and *bayestar* agree to within a factor of a few depending on the S/N threshold used. At S/N 12, the 50th (90th) percentiles agree to within a factor of ~ 3 (~ 8). At S/Ns 15 and 25, this improves to ~ 2 (~ 6) and < 2 (< 6), respectively.

Although localizations largely agree on the event-by-event level, we empirically find that at $\rho_{\text{net}} \lesssim 15$ there are significant biases between the expected localization distributions obtained when compared to *bayestar*. The *pp* plots in Figure 2 show that, in general, the Fisher analysis systematically underestimates the size of the 90% credible sky area. This effect lessens in severity as the S/N threshold is increased. For $\rho_{\text{net}} \geq 25$, the bias has mostly disappeared.

We assert that the statistical agreement between the two methods is trustworthy for systems with $\rho_{\text{net}} \geq 15$, and accurate to $\lesssim 1$ order of magnitude at lower S/Ns. We therefore assume

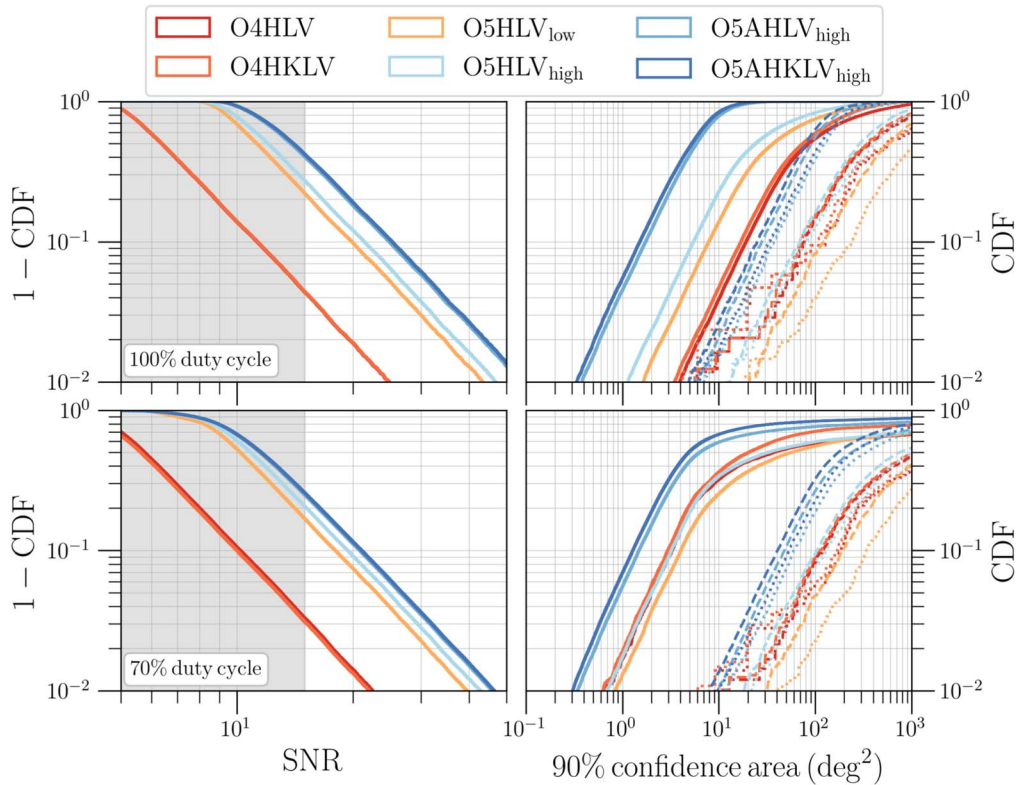


Figure 3. Cumulative S/N (left) and localization (right) distributions for six sample network configurations operating at 100% (top) and 70% (bottom) duty cycles. We include predictions for the early warning localization distributions obtained 0 s (solid), 20 s (dashed), and 40 s (dotted) before a merger. We assume a KAGRA that reaches 25 (125) Mpc sensitivity in the fourth (fifth) observing runs. The 70% duty cycle cumulative distributions assume single detector candidates are not localized (e.g., they are normalized to two or more detector networks). Infrastructure latencies are not included in this plot.

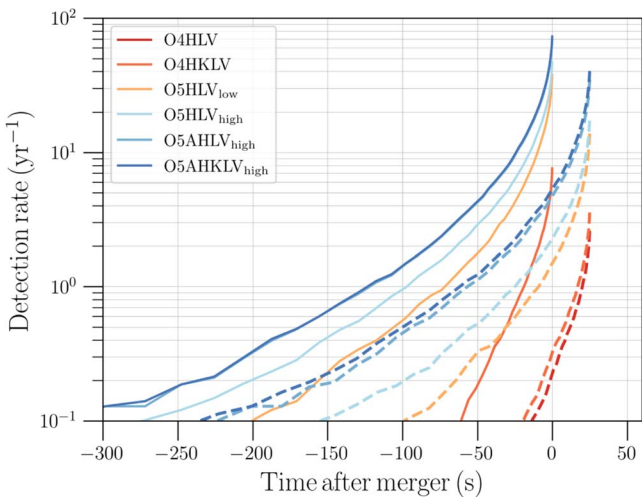


Figure 4. The expected number of detections per year vs. the time detected relative to the merger. The solid (dashed) lines show expectations for six different networks operating at 100% (70%) duty cycle with 0 s (25s) of infrastructure latency. We assume a KAGRA that reaches 25 (125) Mpc sensitivity in the fourth (fifth) observing runs. The solid lines of O4HKLV and O5AHKLV_{high} lie directly on top of the respective networks without KAGRA, O4HLV, and O5AHLV_{high}. All lines assume a median BNS merger rate of 660 $\text{Mpc}^{-3}\text{yr}^{-1}$. We do not include uncertainties associated with that measurement in this plot but note that they will improve (worsen) the expected detections by a factor of ~ 2.5 (~ 0.2).

a localization threshold of $\rho_{\text{net}} \geq 15$ for the remainder of this work and assume the individual localizations produced are accurate to within a factor of a few. At low frequencies, the

Fourier domain representation of the gravitational wave signal changes less rapidly; we therefore expect the resulting derivatives and Fisher matrices to be even more accurate at the reduced bandwidths associated with early warning analyses. The corresponding low-bandwidth comparison between Fisher and *bayestar* localizations can be found in Figure 6 in Appendix, confirming our expectation that the Fisher analysis remains well behaved at truncated frequencies.

4.2. O4

Figures 3 and 4 present the cumulative S/N and localization distributions and the expected yearly early warning detection rates, respectively, for six representative O4 and O5 networks: O4HLV, O4HKLV, O5HLV_{low}, O5HLV_{high}, O5AHLV_{high}, and O5AHKLV_{high}. We highlight two early warning times, 20 and 40 s before a merger, which are motivated by data analysis latencies (Magee et al. 2021) and approximate $\mathcal{O}(10\text{ s})$ slew times.

It was recently announced that KAGRA is expected to join O4 with a horizon of at least $\sim 1\text{ Mpc}$ (LVK 2021). As expected, we find that there is no impact on the network sensitivity and negligible impact on the localizations achieved when this HKLV network is compared to HLV. However, if KAGRA is able to reach 25 Mpc, we find an average $\sim 40\%$ reduction in the 90% credible sky areas for events with $\text{S/N} \geq 15$, though the number of expected detections increases at less than the percent level; see Figure 3. Thus while a moderately sensitive KAGRA in O4 will not increase the

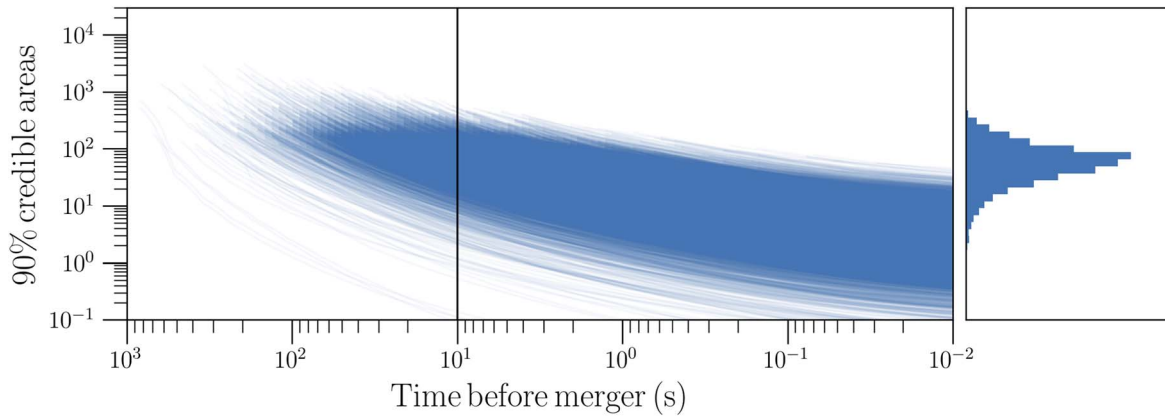


Figure 5. Here we show the expected 90% confidence areas as a function of detected time before a merger for an idealized, design AHKLV network acting at 100% duty cycle. Each line tracks one simulation. The right part shows a histogram of expected localizations at the time indicated by the vertical black line (e.g., 10 s before the merger). At 10 s before the merger, we expect most events to have localizations $\mathcal{O}(100 \text{ deg}^2)$. By the merger, this improves to $\mathcal{O}(1 \text{ deg}^2)$. Simulations are only tracked once a network $S/N \geq 15$ is reached. An animation of this figure that depicts the localization evolution is available online.⁵

(An animation of this figure is available.)

number of detections, it will greatly improve the localization for existing detections.

As shown in Figure 4, early warning alerts in O4 are likely to be exceedingly rare; we expect $\lesssim 1$ detection to be made early enough to overcome analysis latencies per year. Of these observations, we expect 10%–20% to have localizations $\lesssim 100 \text{ deg}^2$. The presence/absence of KAGRA has negligible impact on the localization or abundance of early warning detections.

4.3. O5/Design

For the three-detector HLV network, we find only a moderate $\lesssim 5\%$ difference in the number of detected events above our S/N threshold as the Virgo sensitivity is varied (left column, Figure 3), though the localization distributions noticeably shift. We estimate that up to 20% (13%) of all detected BNSs will have 90% credible sky areas $\lesssim 10 \text{ deg}^2$ for the high (low) sensitivity Virgo projections. We expect up to 16% (8%) of signals detected 20 s early and 13% (4%) of signals detected 40 s early to be localized to $\lesssim 100 \text{ deg}^2$.

LIGO–Aundha has an even larger impact. Its addition to the HLV network suggests we expect up to 80% of detected BNSs to be localized to $\lesssim 10 \text{ deg}^2$ by a merger, dropping to $\lesssim 3\%$ and $\lesssim 1\%$, respectively, 20 s and 40 s before the merger. The addition of KAGRA operating at 125 Mpc has a small impact on both the detection and localization when compared to the AHLV network operating at 100% duty cycle. For this best case network, we also explicitly compute the evolution of the 90% credible sky areas as a function of time before the merger in Figure 5, in addition to the two fiducial early warning times, 20 and 40 s, in Figure 3.

4.4. Duty Cycle Impact on Localizations and Detections

Included in Figure 3 is a comparison of networks operating at 100% versus 70% duty cycle.⁶ The real benefit to networks with a large number of detectors is clear. While at 100% duty cycle there is little difference in localizations produced by four

and five-detector networks, there is a large benefit for networks that can only operate at moderate duty cycles. A four-detector network at 70% duty cycle operates with all four detectors only 24% of the time; for a five-detector network, there are at least four detectors active 53% of the time. The extra detector greatly increases the robustness of the global detector network. This effect is well demonstrated by the O5AHLV_{high} and O5AHKLV_{high} curves in the right panels of Figure 3.

The impact on detection is also easily visualized. Figure 4 shows the expected number of detections at a fiducial BNS rate⁷ of $660_{-530}^{+1040} \text{ Gpc}^{-3} \text{ yr}^{-1}$ for networks operating at 100% and 70% duty cycles, respectively. In all scenarios considered, down time decreases the total number of expected detections by a factor of a few.

5. Outlook and Discussion

Early warning detection will facilitate the capture of prompt, rapidly fading emission associated with BNS mergers. We find that even the most optimistic scenarios for O4 predict ~ 1 BNS detected before a merger per year, with localizations $\gtrsim 100 \text{ deg}^2$. These detections will likely be too poorly localized for optical facilities to follow up. We expect wide-field observatories such as the Murchinson Wide Field Array (Tingay et al. 2013) and the space-based Fermi Gamma-ray Burst Monitor (Meegan et al. 2009) and the Neil Gehrels Swift Observatory (Gehrels et al. 2004) to benefit most from early warning detection with poor localizations. Indeed, new observational modes enabled with the Murchinson Wide Field Array will allow tests of BNSs as possible progenitors of nonrepeating fast radio bursts (James et al. 2019), and will probe longstanding predictions tying fast radio bursts to premerger magnetosphere interactions (Hansen & Lyutikov 2001).

Swift’s ability to rapidly localize will facilitate observations of near-merger X-ray emission, and recent Swift/BAT updates (Tohuvavohu et al. 2020) will enable subthreshold gamma-ray burst detections. Prompt X-ray observations could help reveal the immediate aftermath of the coalescing objects, and subthreshold detections could identify off-axis gamma-ray

⁵ <https://dcc.ligo.org/public/0180/P2200010/002/movie>

⁶ Chosen to match the duty cycle in the LVK’s observing scenario document (Abbott et al. 2021e).

⁷ We choose the BNS rate corresponding to the multi source model (MS) model described in Abbott et al. (2021e) since our population most closely matches that distribution.

bursts and help probe the jet structure associated with these mergers. Similarly, observations by the Fermi Large Area Telescope would help complete our understanding of high-energy gamma-ray emission; in fact the telescope had powered down just before GRB 170817A, which occluded measurements at energies $\gtrsim 100$ MeV (Kocevski et al. 2017).

By O5, early warning detections will become more common with ~ 6 alerts distributed before a merger per year. Depending on network configuration and duty cycle, we expect that up to 80% of these will be localized to $\lesssim 10$ deg², making them a prime target for optical facilities that cover $\mathcal{O}(1-10)$ deg², such as the Zwicky Transient Facility (Graham et al. 2019), Dark Energy Camera (Flaugher et al. 2015), and the highly anticipated Vera C. Rubin Observatory (Ivezic et al. 2019). Although previous optical observations were able to capture the kilonova associated with GW170817, it was already fading and clouded a complete understanding of the nature of the blue ejecta (Cowperthwaite et al. 2017; Nicholl et al. 2017). Chase et al. (2022) provide an in depth review of kilonova detectability prospects across multiple observing bands for a selection of current and planned wide field-of-view observatories.

Other works have also estimated sensitivities and localization prospects for early warning detection of BNSs for specific sensitivities and 100% duty cycles. We find that when our S/N detection threshold is modified to match those works, we obtain similar results in the 100% duty cycle limit. Sachdev et al. (2020) considered a HLV network operating at design sensitivity, finding that $\mathcal{O}(0.1 - 1)\%$ of all detected BNS events will be detected early with localizations $\lesssim 100$ deg². If we impose a detection threshold of S/N 10, corresponding to the top 99% of recovered events in their study, we obtain similar expected localizations. Nitz et al. (2020a) also considered HLV, HKLV, and AHKLV networks from the “design” to “voyager” eras of ground-based detectors. We find that the distributions we present in Figure 3 for the O5HLV and O5AHLV networks are consistent with the distributions they find at S/N 10 in their Figure 3. This is complicated by the fact that we use slightly different sensitivity curves.

The observing scenarios document most recently produced by the LVK (Abbott et al. 2020b) does not consider early warning prospects, but we can compare our 0 s early prospects to theirs. Their predictions for O4 considered the same HKLV network at 70% duty cycle with one major difference: KAGRA was assumed to reach 80 Mpc sensitivity; $\sim 40\%$ ($\sim 14\%$) of detected events were predicted to have 90% credible sky areas smaller than 20 (5) deg². We find that this matches our predictions in the bottom right panel of Figure 3, which assumes a detection threshold of S/N 15 and a duty cycle of

70%. If we drop our S/N threshold to 12 to match the observing scenario document, we find slightly poorer constraints, likely attributable to the less sensitive KAGRA used in our network.

Although our results agree with similar studies, we caution that the specifics of the predicted distributions are highly dependent on the S/N threshold used for recovery. As shown in Section 4.1, we expect this method to consistently agree to within a factor of a few at the 50% level though Figure 2 shows that there is bias in the predicted distribution. Our detection threshold of 15 ensures that we (1) conservatively estimate the detection rate and (2) obtain reasonably accurate localization distributions. We have limited our study to the current generation of ground-based detectors, but others have considered early warning prospects for networks that include Cosmic Explorer and the Einstein Telescope (Chan et al. 2018; Akcay 2019; Nitz & Dal Canton 2021). We leave further studies of these configurations to future work.

LIGO was constructed by the California Institute of Technology and Massachusetts Institute of Technology with funding from the National Science Foundation and operates under cooperative agreement PHY-1764464. This paper carries LIGO document number LIGO-P2200010. The authors are grateful for computational resources provided by the LIGO Laboratory and supported by National Science Foundation grants PHY-0757058 and PHY-0823459. S.B. further acknowledges support from the Deutsche Forschungsgemeinschaft (DFG), project MEMI number BE6301/2-1, and NSF grant PHY-1836779. We thank Surabhi Sachdev for providing a careful review of this manuscript, and BS Sathyaprakash for useful comments. R.M. gratefully acknowledges productive conversations with Shreya Anand and Derek Davis.

Appendix

Sky Localization Comparison at Reduced Bandwidth

Figure 6 shows the comparison of the 90% credible sky areas computed with *bayestar* and Fisher analysis for reduced bandwidths with upper frequency cutoffs of 49 and 56 Hz, respectively, for two S/N thresholds of 12 and 15. We do not consider an S/N threshold of 25 due to the low number of early warning signals that reach this threshold. As expected, the comparison shows a better agreement between the two methods than at full bandwidth, validating our use of the Fisher analysis for both full bandwidth and early warning signals.

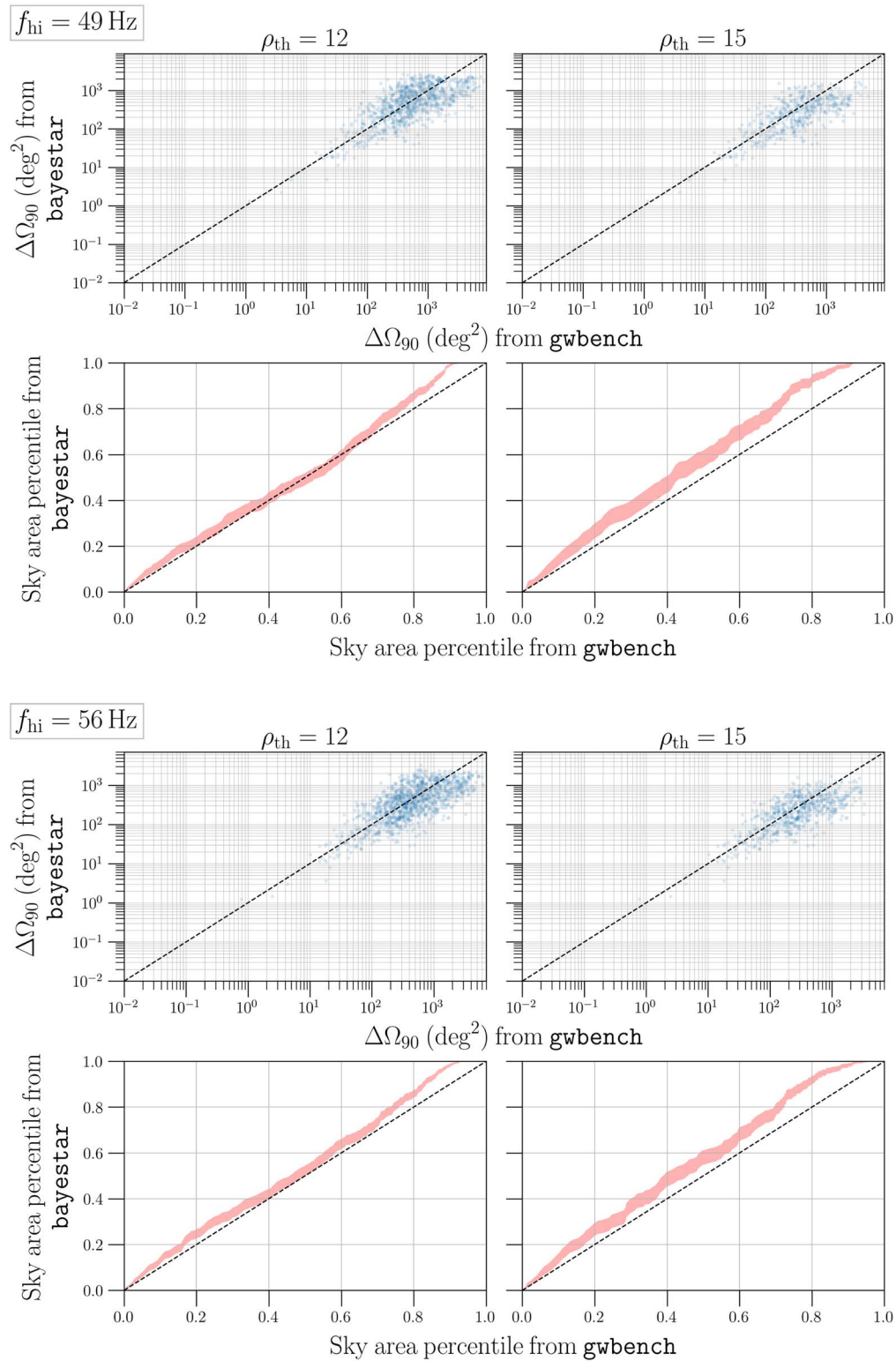


Figure 6. A comparison of the 90% confidence interval computed by bayestar vs. the Fisher matrix formalism used here (gwbench) analogous to Figure 2 but at reduced bandwidths due to smaller upper frequency cutoffs, f_{hi} , of 49 and 56 Hz instead of 1024 Hz. We only present the results for S/N thresholds ρ_{th} 12 and 15 due to the low number of events surpassing an S/N threshold of $\rho_{th} = 25$ at reduced bandwidths. All localizations are computed assuming 100% duty cycle and design sensitivity estimates. At a lower bandwidth we do not find that gwbench systematically underestimates the size of the confidence interval at S/N 12.

ORCID iDs

Ryan Magee  <https://orcid.org/0000-0001-9769-531X>
 Ssohrab Borhanian  <https://orcid.org/0000-0003-0161-6109>

References

Aasi, J., Abadie, J., Abbott, B P, et al. 2015, *CQGr*, 32, 074001
 Abbott, B. P., Abbott, R., Abbott, T. D., et al. 2016, *PhRvL*, 116, 061102
 Abbott, B. P., Abbott, R., Abbott, T. D., et al. 2017a, *PhRvL*, 119, 161101

- Abbott, B. P., Abbott, R., Abbott, T. D., et al. 2017b, *ApJL*, **848**, L12
- Abbott, B. P., Abbott, R., Abbott, T. D., et al. 2019, *PhRvX*, **9**, 031040
- Abbott, B. P., Abbott, R., Abbott, T. D., et al. 2020a, *ApJL*, **892**, L3
- Abbott, B. P., Abbott, R., Abbott, T., et al. 2020b, *LRR*, **23**, 1
- Abbott, R., Abbott, T. D., Abraham, S., et al. 2021a, *PhRvX*, **11**, 021053
- Abbott, R., Abbott, T. D., Abraham, S., et al. 2021d, *ApJL*, **915**, L5
- Abbott, R., Abbott, T. D., Acernese, F., et al. 2021b, arXiv:2108.01045
- Abbott, R., Abbott, T. D., Acernese, F., et al. 2021c, arXiv:2111.03606
- Abbott, R., Abbott, T. D., Acernese, F., et al. 2021e, arXiv:2111.03634
- Acernese, F., Agathos, M., Agatsuma, K., et al. 2015, *CQGra*, **32**, 024001
- Akcaay, S. 2019, *Annalen Phys*, **531**, 1800365
- Akutsu, T., Ando, M., Arai, K., et al. 2019, *NatAs*, **3**, 35
- Ashton, G., Hübner, M., Lasky, P., et al. 2019, *ApJS*, **241**, 27
- Balasubramanian, R., Sathyaprakash, B., & Dhurandhar, S. 1996, *PhRvD*, **54**, 3033
- Barack, L., & Cutler, C. 2004, *PhRvD*, **69**, 082005
- Berry, C. P. L., Mandel, I., Middleton, H., et al. 2015, *ApJ*, **804**, 114
- Blanchet, L., Damour, T., Esposito-Farese, G., & Iyer, B. R. 2005, *PhRvD*, **71**, 124004
- Blanchet, L., Damour, T., Iyer, B. R., Will, C. M., & Wiseman, A. 1995, *PhRvL*, **74**, 3515
- Borhanian, S. 2021, *CQGra*, **38**, 175014
- Borhanian, S., & Sathyaprakash, B. S. 2022, arXiv:2202.11048
- Buonanno, A., Iyer, B., Ochsner, E., Pan, Y., & Sathyaprakash, B. S. 2009, *PhRvD*, **80**, 084043
- Cannon, K., Cariou, R., Chapman, A., et al. 2012, *ApJ*, **748**, 136
- Chan, M. L., Messenger, C., Heng, I. S., & Hendry, M. 2018, *PhRvD*, **97**, 123014
- Chase, E. A., O'Connor, B., Fryer, C. L., et al. 2022, *ApJ*, **927**, 163
- Chu, Q., Howell, E. J., Rowlinson, A., et al. 2016, *MNRAS*, **459**, 121
- Cowperthwaite, P. S., Berger, E., Villar, V. A., et al. 2017, *ApJL*, **848**, L17
- Cutler, C. 1998, *PhRvD*, **57**, 7089
- Cutler, C., & Flanagan, E. E. 1994, *PhRvD*, **49**, 2658
- Evans, M., Adhikari, R., Afle, C., et al. 2021, arXiv:2109.09882
- Fairhurst, S. 2009, *NJPh*, **11**, 123006
- Finn, L. S. 1992, *PhRvD*, **46**, 5236
- Finn, L. S., & Chernoff, D. F. 1993, *PhRvD*, **47**, 2198
- Flaugher, B., Diehl, H. T., Honscheid, K., et al. 2015, *AJ*, **150**, 150
- Foucart, F., Duez, M. D., Kidder, L. E., et al. 2019, *PhRvD*, **99**, 103025
- Foucart, F., Hinderer, T., & Nissanke, S. 2018, *PhRvD*, **98**, 081501
- Gehrels, N., Chincarini, G., Giommi, P., et al. 2004, *ApJ*, **611**, 1005
- Graham, M. J., Kulkarni, S. R., Bellm, E. C., et al. 2019, *PASP*, **131**, 078001
- Hansen, B. M. S., & Lyutikov, M. 2001, *MNRAS*, **322**, 695
- Ivezic, V., Kahn, S., Tyson, J., et al. 2019, *ApJ*, **873**, 111
- Iyer, B., et al. 2011, LIGO India, Tech. Rep. LIGO-M1100296, <https://dcc.ligo.org/LIGO-M1100296/public>
- James, C. W., Anderson, G. E., Wen, L., et al. 2019, *MNRAS Lett.*, **489**, L75
- Kocevski, D., Omodei, N., & Vianello, G. 2017, arXiv:1710.05450
- Kovalam, M., Patwary, M. A. K., Sreekumar, A. K., et al. 2022, *ApJL*, **927**, L9
- Li, Y., Heng, I. S., Chan, M. L., Messenger, C., & Fan, X. 2022, *PhRvD*, **105**, 043010
- LVK 2021, O4 Observing Plan Update, <https://www.ligo.org/scientists/GWEMalerts.php>
- LVK 2022, LIGO-T2000012: publicly provided PSDs from latest observing scenario
- Magee, R., Fong, H., Caudill, S., et al. 2019, *ApJL*, **878**, L17
- Magee, R., Chatterjee, D., Singer, L., et al. 2021, *ApJL*, **910**, L21
- Meegan, C., Lichti, G., Bhat, P. N., et al. 2009, *ApJ*, **702**, 791
- Nicholl, M., Berger, E., Kasen, D., et al. 2017, *ApJL*, **848**, L18
- Nitz, A. H., Capano, C., Nielsen, A. B., et al. 2019, *ApJ*, **872**, 195
- Nitz, A. H., Capano, C. D., Kumar, S., et al. 2021, *ApJ*, **922**, 76
- Nitz, A. H., & Dal Canton, T. 2021, *ApJL*, **917**, L27
- Nitz, A. H., Schäfer, M., & Dal Canton, T. 2020a, *ApJL*, **902**, L29
- Nitz, A. H., Dent, T., Davies, G. S., et al. 2020b, *ApJ*, **891**, 123
- Olsen, S., Venumadhav, T., Mushkin, J., et al. 2022, arXiv:2201.02252
- Özel, F., & Freire, P. 2016, *ARA&A*, **54**, 401
- Pankow, C., Rizzo, M., Rao, K., Berry, C. P. L., & Kalogera, V. 2020, *ApJ*, **902**, 71
- Poisson, E., & Will, C. M. 1995, *PhRvD*, **52**, 848
- Rodriguez, C. L., Farr, B., Farr, W. M., & Mandel, I. 2013, *PhRvD*, **88**, 084013
- Sachdev, S., Magee, R., Hanna, C., et al. 2020, *ApJL*, **905**, L25
- Saleem, M., Rana, J., Gayathri, V., et al. 2022, *CQGra*, **39**, 025004
- Sathyaprakash, B. S., & Dhurandhar, S. V. 1991, *PhRvD*, **44**, 3819
- Singer, L. P., & Price, L. R. 2016, *PhRvD*, **93**, 024013
- Singer, L. P., Price, L., Farr, B., et al. 2014, *ApJ*, **795**, 105
- Singh, M. K., Kapadia, S. J., Shaikh, M. A., Chatterjee, D., & Ajith, P. 2021, *MNRAS*, **502**, 1612
- Tingay, S. J., Goeke, R., Bowman, J. D., et al. 2013, *PASA*, **30**, e007
- Tohuvavohu, A., Kennea, J. A., DeLaunay, J., et al. 2020, *ApJ*, **900**, 35
- Trovato, A. 2020, in PoS, Asterics2019, 357 (Trieste: SISSA), 082
- Tsutsui, T., Nishizawa, A., & Morisaki, S. 2022, *MNRAS*, **512**, 3878
- Vallisneri, M. 2008, *PhRvD*, **77**, 042001
- Veitch, J., Raymond, V., Farr, B., et al. 2015, *PhRvD*, **91**, 042003
- Venumadhav, T., Zackay, B., Roulet, J., Dai, L., & Zaldarriaga, M. 2020, *PhRvD*, **101**, 083030
- Washimi, T., Yokozawa, T., Tanaka, T., et al. 2021, *CQGra*, **38**, 125005
- Yu, H., Adhikari, R. X., Magee, R., Sachdev, S., & Chen, Y. 2021, *PhRvD*, **104**, 062004
- Zackay, B., Venumadhav, T., Dai, L., Roulet, J., & Zaldarriaga, M. 2019, *PhRvD*, **100**, 023007